THE ASTROPHYSICAL JOURNAL, 328:734–746, 1988 May 15

AN ANALYSIS OF THE SHAPES OF ULTRAVIOLET EXTINCTION CURVES. II. THE FAR-UV EXTINCTION

EDWARD L. FITZPATRICK[1]
Joint Institute for Laboratory Astrophysics, University of Colorado and National Bureau of Standards

AND

DERCK MASSA[1]
Applied Research Corporation
Received 1987 July 24; accepted 1987 November 3

ABSTRACT

In this paper we examine the properties of interstellar extinction in the far-ultraviolet region (FUV; $\lambda <$ 1700 Å) utilizing *IUE* extinction curves for a primary data sample of 45 reddened Milky Way OB stars. These results are combined with those derived for the 2175 Å bump in a previous study. We find that *IUE* extinction curves can be represented by linear combinations of a Lorentzian-like 2175 Å bump profile, a well-determined FUV curvature term, and an underlying linear component. The parameters of the linear component (i.e., slope and intercept) are strongly correlated and therefore only five free parameters are required to fit all of the curves in our sample. Three parameters describe the 2175 Å bump (centroid, width, and strength), one parameter describes the linear background (either slope or intercept), and one parameter describes the strength of the FUV curvature term. The *shape* of the FUV curvature is found to be identical, to within the observational errors, for all the curves in our sample—which spans virtually the entire range of extinction curve morphologies observed in the Milky Way. This implies that the curvature component is not an artifact of the size distribution or relative combinations of the absorbing particles, but is rather a distinct optical property of some physical dust component. We suggest that the FUV curvature seen in the *IUE* curves represents the long-wavelength tail of a FUV resonance, analogous to the 2175 Å bump.

Subject headings: interstellar: matter — ultraviolet: spectra

I. INTRODUCTION

This is the second in a series of papers examining the shapes of ultraviolet interstellar extinction curves and their variations. Relationships among factors which describe the shapes of the curves furnish constraints on the properties and constituents of interstellar grains. Fitzpatrick and Massa (1986; hereafter Paper I) demonstrated that excellent fits to the shape of the 2175 Å extinction bump, as observed with the *International Ultraviolet Explorer* (*IUE*) satellite, could be obtained using a functional form referred to as the "Drude profile." This function is similar to a Lorentzian but is more easily interpreted as an absorption cross section of solids (Bohren and Huffman 1983). The main results from Paper I are that the observed extinction bumps span a wide range in FWHM values, from $\sim$360 to $\sim$600 Å, but show only small positional variations. The mean position of the peak was found to be 2174.4 Å, with an extreme range of only $\pm$17 Å about the mean. We also found that the bump width is strongly correlated with the dust grain environments. Grains in dense regions produce broad bumps, while grains in diffuse regions and regions of recent early-type star formation produce narrower ones. The impact of these results on current theories of the origin of the bump were discussed in Paper I.

In the present paper we examine the properties of the far-ultraviolet (FUV) extinction and, in particular, its relationship with the 2175 Å bump. The data set used here is described in § II. In § III we investigate the shapes of the FUV portion of extinction curves and show that all *IUE* extinction curves in our sample can be represented by a simple fitting function consisting of six free parameters. Correlations among the parameters and between the parameters and the extinction environments are presented in § IV. We discuss our results in § V and interpret them within the framework of a simple physical model.

II. THE DATA

The main data set for this study consists of ultraviolet extinction curves derived for 45 reddened Milky Way stars observed in the low-dispersion mode of the *IUE* satellite (Boggess *et al.* 1978*a*, *b*). The stars, their spectral types, their $E(B-V)$ values, and the original reference to their extinction curves are listed in columns (1)–(5) of Table 1. The type of environment in which the extinction arises is noted in column (6). Additional spectroscopic and photometric data will be given by Fitzpatrick and Massa (1988; hereafter Paper III), where all the data for this project will be compiled and displayed. The selection criteria for the 45 reddened Milky Way stars are discussed in Paper I. The extinction curves were produced, using the pair method, as described by Massa and Fitzpatrick (1986; hereafter MF). The stars used as flux standards will be listed in Paper III along with their spectroscopic and photometric data. Before the extinction curves were constructed, all the reddened stars were corrected for their strong interstellar Lyα absorption

[1] Guest Observer with the *International Ultraviolet Explorer* satellite, which is sponsored and operated by the National Aeronautics and Space Administration, the Science Research Council of the United Kingdom, and the European Space Agency.

TABLE 1

EXTINCTION CURVE DATA

HD (E) or BD	Name	Spectral type	E(B-V)	Environment type[a]	Original curve source[b]	Curve Fit Coefficients					
						λ_0^{-1}	γ	c_1	c_2	c_3	c_4
13338	---	B1 V	0.51	DIF	WBS	4.594	0.939	-0.032	0.794	3.977	0.377
14250	Oo1586	B1 III	0.57	DIF	---	4.570	0.950	-0.235	0.794	4.129	0.396
21483	---	B3 III	0.55	DEN	---	4.631	1.011	-0.278	0.730	2.368	0.658
34078	AE Aur	09.5 V	0.53	DEN	WBS	4.589	1.087	0.473	0.571	4.152	0.520
36982	LP Ori	B2 V	0.34	DEN	Pan	4.575	0.873	1.101	0.050	2.638	0.311
37022	θ^1 Ori C	06 p	0.34	STF	BoS	4.635	0.846	1.251	0.033	1.331	0.186
37023	θ^1 Ori D	B0.5	0.37	STF	BoS	4.594	0.878	1.883	-0.083	1.214	0.153
37061	NU Ori	B0.5 Vp	0.54	DEN	Pan	4.581	1.074	1.309	0.109	2.041	0.044
37367	---	B2 IV-V	0.40	DIF	MSF	4.601	0.901	0.708	0.555	3.985	0.260
37903	---	B1.5 V	0.35	DEN	MSF	4.615	1.045	0.965	0.384	3.300	0.440
38087	---	B3 n	0.33	DEN	WBS	4.563	1.026	1.137	0.230	4.508	0.310
38131	---	B0.5 V	0.49	DIF	WBS	4.608	0.955	-0.174	0.755	3.707	0.332
46056	---	08 Vn	0.51	DIF	---	4.611	0.932	-0.527	0.857	3.032	0.541
46202	---	09 V	0.47	DIF	---	4.599	0.842	-0.348	0.864	2.542	0.515
48099	---	07 V	0.27	DIF	Sea	4.576	0.831	-0.856	0.874	2.978	0.339
73882	---	08.5 V((n))	0.72	DEN	MSF	4.576	1.192	-0.412	0.788	3.342	0.540
91824	---	07 V((f))	0.27	DIF	---	4.604	0.917	0.195	0.633	2.894	0.473
93028	---	09 V	0.24	DIF	---	4.637	0.839	-0.757	0.811	1.557	0.166
93222	---	07 III((f))	0.40	DIF	---	4.577	0.804	-0.053	0.626	1.697	0.236
147701	---	B5 V	0.73	DEN	Sea	4.615	1.135	1.290	0.329	3.582	0.888
147888	ρ Oph D	B3 V:	0.52	DEN	Sea	4.587	1.022	1.611	0.133	3.823	0.339
147889	---	B2 V	1.09	DEN	BoS	4.617	1.082	1.449	0.151	4.472	0.709
147933/4	ρ Oph AB	B2 IV+V	0.47	DEN	BlS	4.594	0.969	1.642	0.139	3.349	0.349
149757	ζ Oph	09.5 V	0.32	DEN	BlS	4.595	1.383	-0.802	0.900	5.842	0.563
154445	---	B1 V	0.42	DEN	Sea	4.568	1.058	1.098	0.309	5.034	0.503
167771	---	07 III:(n)((f))	0.44	DEN	Sea	4.561	0.974	-0.139	0.574	3.448	0.453
185418	---	B0.5 V	0.50	DEN	Sea	4.579	0.927	1.266	0.362	3.941	0.381
193322	---	09 V:((n))	0.41	DIF	---	4.613	0.856	-0.617	0.879	2.264	0.115
197512	---	B1 V	0.32	DIF	WBS	4.585	1.006	-1.043	1.021	4.659	0.438
199579	---	06 V((f))	0.37	DIF	Sea	4.606	0.997	-0.725	0.898	2.923	0.453
203938	---	B0.5 IV	0.74	DEN	Sea	4.589	1.016	0.087	0.747	3.647	0.306
204827	---	B0 V	1.11	DEN	WBS	4.623	1.077	-1.521	1.219	3.201	0.899
229196	---	06 III(n)(f)	1.22	DIF	MSF	4.581	0.990	-0.179	0.728	3.407	0.233
239729	---	B0 V	0.66	DIF	---	4.605	1.076	0.076	0.728	3.391	0.685
251204	---	B1 V	0.78	DIF	MSF	4.594	0.893	-0.672	0.861	2.862	0.383
252325	---	B0 IV	0.87	DEN	MSF	4.617	0.914	1.048	0.387	2.881	0.484
+56 524	Oo1078	B1 Vn	0.60	DIF	---	4.577	1.023	-0.690	0.916	4.027	0.496
+57 513	---	B1 III	0.54	DIF	WBS	4.589	0.909	-0.920	0.920	3.332	0.373
+59 562	---	08 V	0.79	DIF	MMN	4.595	0.907	-0.322	0.755	2.973	0.352
+60 594	---	09 V	0.66	DIF	MMN	4.594	0.932	-0.548	0.819	3.457	0.410

TABLE 1—*Continued*

HD (E) or BD	Name	Spectral type	E(B-V)	Environment type[a]	Original curve source[b]	Curve Fit Coefficients					
						λ_0^{-1}	γ	c_1	c_2	c_3	c_4
-59 2600	---	06 V((f))	0.53	DIF	---	4.594	0.950	0.087	0.601	2.448	0.179
---	Herschel 36	07.5 V(n)	0.89	STF	HHW	4.620	0.886	1.680	0.055	1.998	0.312
---	Hiltner 188	B1 V	0.68	DIF	MMN	4.603	0.934	-1.064	0.989	3.316	0.469
---	Oo936	B1.5 V	0.55	DIF	---	4.584	0.921	-0.411	0.902	3.638	0.531
---	Tr 14 #20	06 V	0.60	DIF	---	4.581	0.890	-0.180	0.729	2.287	0.383
NGC2244 Average		---	---	---	MF	4.596	0.877	0.053	0.646	3.090	0.465
NGC3293 Average		---	---	---	MF	4.603	0.976	-0.061	0.719	3.019	0.406
NGC6231 Average		---	---	---	MF	4.596	0.970	0.060	0.684	3.440	0.385
Cepheus OB3 Average		---	---	---	MF	4.597	0.988	0.192	0.616	3.640	0.474
Trumpler 14 Average		---	---	---	MF	4.583	0.955	0.140	0.560	2.635	0.356
LMC Average		---	---	---	Fit	4.608	0.994	-0.687	0.891	2.550	0.504
30 Doradus Average		---	---	---	Fit	4.606	0.984	-2.186	1.388	1.488	0.425
Seaton Galactic Average		---	---	---	Stn	4.595	1.051	-0.384	0.739	3.961	0.265

[a] DIF, diffuse interstellar medium; DEN, dense interstellar medium; STF, region of recent early-type star formation.

[b] WBS, Witt *et al.* 1984; Pan, Panek 1983; BoS, Bohlin and Savage 1981; MSF, Massa *et al.* 1983; Sea, Seab 1982; BlS, Bless and Savage 1972; MMN, Morgan *et al.* 1982; MF, Massa and Fitzpatrick 1986; Fit, Fitzpatrick 1986; Stn, Seaton 1979.

lines using damped absorption line profiles. The resultant extinction curves are thus unaffected by Lyα absorption, although the region 1200–1230 Å is still unusable due to lack of signal and the presence of geocoronal Lyα emission.

The H I column densities were taken from the literature for some of the stars, but most were derived by us through profile fitting the strong damping wings of Lyα in the low-dispersion *IUE* spectra using the method of Bohlin (1975). This method was adapted to the low-dispersion data by smearing the theoretical line profiles with a 6 Å Gaussian (the *IUE* instrumental profile). In addition, a systematic 2–3 Å error in the SWP low-dispersion wavelength calibration was noted (in the sense that 1215 Å is shifted to $\sim$1213 Å on the *IUE* scale) and compensated for by placing the centers of the theoretical profiles at the locations of the measured centers of the interstellar absorption lines—rather than at an *IUE* wavelength of 1215.7 Å. We have found that column densities measured from the low-dispersion data always agree to within $\pm$40% of column densities reported from *Copernicus* or high-dispersion *IUE* measurements (which are typically claimed to have $\pm$25% accuracy). The H I column densities for the stars in our sample, and their sources, will be given in Paper III.

Our data set also includes the extinction curves for stars in the five Milky Way open clusters discussed by MF and the two Large Magellanic Cloud (LMC) extinction curves derived by Fitzpatrick (1986). MF used the cluster extinction data in a detailed examination of the accuracy of *IUE* extinction curves. The results and methodology of that study are used here to examine the significance of our results. The two LMC extinction curves represent the average extinction properties of stars located within 0°.5 from the center of the 30 Doradus nebula (referred to as the "30 Dor regional curve") and of stars located in a variety of LMC regions well away from 30 Doradus (referred to as the "LMC average curve").

III. EXTINCTION CURVE PARAMETRIZATION

In this section we develop a parametrization scheme which reproduces the *IUE* ultraviolet extinction curves obtained from Milky Way and LMC lines of sight. First, we examine the wavelength dependence of extinction at wavelengths shortward of 1700 Å (§ III*a*). This information is then used to parametrize the curve over the wavelength range $\sim$1200–3000 Å (§ III*b*).

a) The Wavelength Dependence of Extinction at $\lambda < 1700$ Å

In Paper I we noted that the excellence of the Drude profile fits to the 2175 Å bump strongly suggests that the underlying, or background, extinction does not deviate substantially from linear (in λ^{-1}) in the region of the fits ($3.3 < \lambda^{-1} < 5.9\ \mu m^{-1}$). This point is illustrated in Figure 1, where we show a number of curves from which the best-fit Drude profiles (as determined in Paper I) have been subtracted. The extinction curves have been binned in 0.05 μm^{-1} intervals, and the spectral mismatch blemishes (e.g., C IV at $\lambda^{-1} \approx 6.5\ \mu m^{-1}$) and the 1200–1230 Å region have been removed. The Drude profiles were extrapolated over the entire lengths of the curves and then subtracted, although the fitting region was only between 3.3 and 5.9 μm^{-1} (indicated by the vertical tick marks at the top and bottom of Fig. 1). The curves do not show any sudden change in slope at the boundary of the fitting region, and some appear linear over a much wider interval (note particularly HD 193322). This, and the high quality of the Drude profile fits, is consistent with the hypothesis that the linear background is not an arbitrary artifact of the bump fitting process, although, as noted in Paper I, we cannot rule out low-frequency departures from linearity.

The residual curvature in the ultraviolet portions of the "debumped" curves is typically not apparent in our sample until wavelengths shortward of $\sim$7 μm^{-1} ($\sim$1430 Å). The wavelength dependence of the curvature can be examined further by removing the linear components which result from the bump fitting process from the curves. We selected 18 curves, which have well-determined FUV extinction properties, span a wide range of curve types and originate in a wide variety of interstellar environments. The Drude profiles and the linear components determined in Paper I were extrapolated and subtracted off these curves. The residual curves, which consist of the isolated FUV curvature components, were then averaged together. Figure 2*a* shows the 18 individual curves superposed. Each curve has been scaled by a one-parameter least-squares fit to the 18 curve average. (The curves used in Fig. 2*a* are listed in the figure legend.) The surprising result in Figure 2*a* is that the wavelength dependence of the FUV curvature is apparently the same for all 18 curves. This is particularly interesting because of the range of interstellar environments represented. The data in Figure 2*a* and the results of the fitting procedure described in § III*b* lead us to one of the main observational results of this paper, namely, to within our measurement errors, the wavelength dependence of the FUV curvature can be satisfactorily fitted by the same function. This is not to say that all the curves necessarily have identical FUV curvature, but whatever intrinsic variations do exist are probably small. The major differences in the appearances of the curves result from differences in the slope of the underlying linear component and differences in the "amount" of the curvature component present.

The wavelength dependence of this FUV curvature component can be quantified by fitting a polynomial to the 18 curve average described above. The average and the fit are shown in Figure 2*b*. The polynomial fit is given by

$$F(\lambda^{-1}) = \begin{cases} 0.5392(\lambda^{-1} - 5.9)^2 + 0.0564(\lambda^{-1} - 5.9)^3 & \text{for } \lambda^{-1} > 5.9\ \mu m^{-1}, \\ 0.0 & \text{for } \lambda^{-1} < 5.9\ \mu m^{-1}. \end{cases} \quad (1)$$

b) Parameterization of Ultraviolet Extinction Curves

The results of Paper I and § III*a* imply that *IUE* extinction curves can be expressed as linear combinations of a Drude bump profile, a linear background, and the FUV curvature function, $F(\lambda^{-1})$. This fitting function is given by

$$\frac{E(\lambda - V)}{E(B - V)} = c_1 + c_2 \lambda^{-1} + c_3 D(\lambda^{-1}, \gamma, \lambda_0^{-1}) + c_4 F(\lambda^{-1}), \quad (2)$$

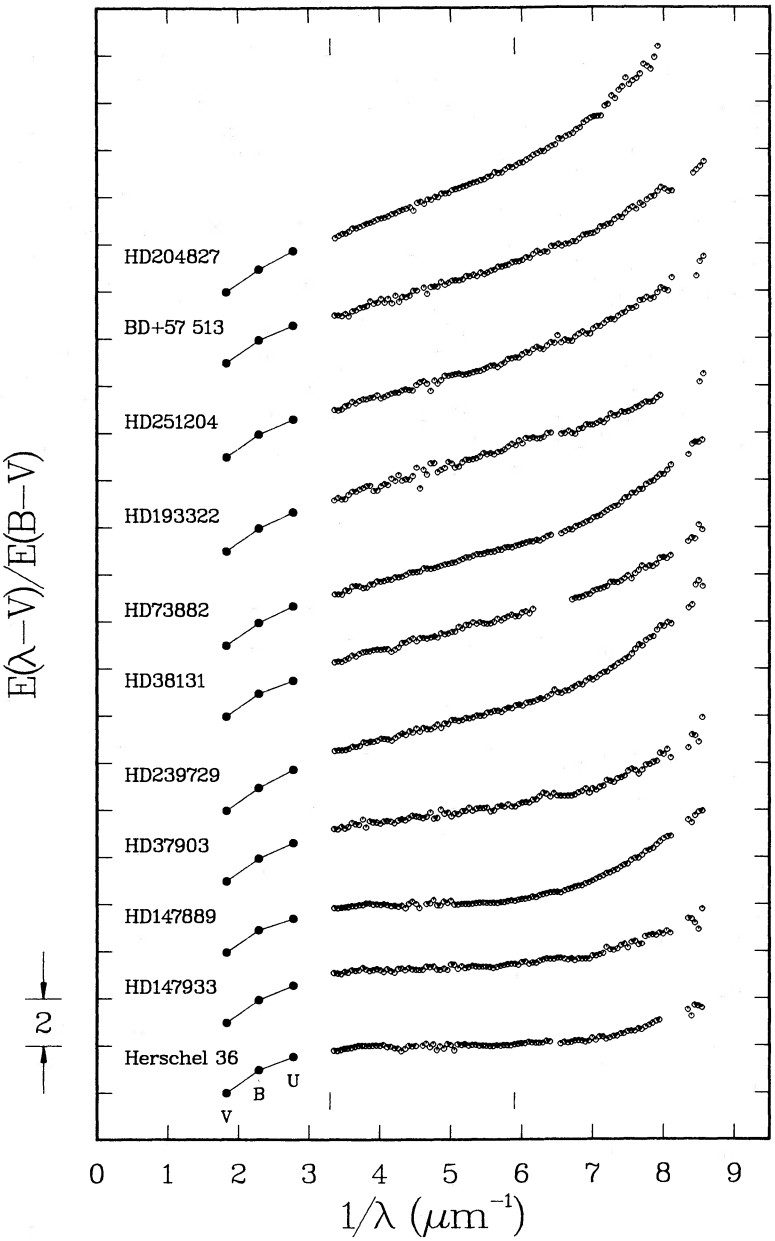

FIG. 1.—Examples of "debumped" interstellar extinction curves. The fitting function to the 2175 Å bump—the "Drude profile"—has been extrapolated over the range 1.8–8.5 μm^{-1} (5500–1200 Å) and subtracted from each curve. The parameters of the Drude profiles are as given in Paper I and were determined by fitting the Drude profile to the observed extinction curves over the region 3.3–5.9 μm^{-1} (see the vertical tick marks at the top and bottom of the figure). The extinction curves consist of *UBV* photometry (*filled circles*) and *IUE* spectrophotometry binned in 0.05 μm^{-1} intervals (*open circles*).

where $D(\lambda^{-1}, \gamma, \lambda_0^{-1})$ is the Drude profile

$$D(\lambda^{-1}, \gamma, \lambda_0^{-1}) = \frac{\lambda^{-2}}{(\lambda^{-2} - \lambda_0^{-2})^2 + \gamma^2 \lambda^{-2}}, \tag{3}$$

and $F(\lambda^{-1})$ is defined in § III*a* (eq. [1]). Six parameters determine each curve—three defining the Drude profile (c_3, γ, λ_0^{-1}), two defining the linear background (c_1, c_2), and one describing the strength of the FUV curvature (c_4).

For each *IUE* extinction curve, the six parameters were determined simultaneously using equation (2) and standard least-squares grid search techniques. The fitting was performed over the whole wavelength range of the curves, typically 3.3–8.5 μm^{-1}. The fit parameters for the 45 Milky Way curves in our sample are sample are listed in Table 1, columns (7)–(12). Fit parameters are also given for the Seaton (1979) average Galactic curve, for the two LMC extinction curves (Fitzpatrick 1986), and for the mean extinction curves for the Milky Way clusters studied by MF. Fit parameters for the individual curves in MF's study will be given in Paper III.

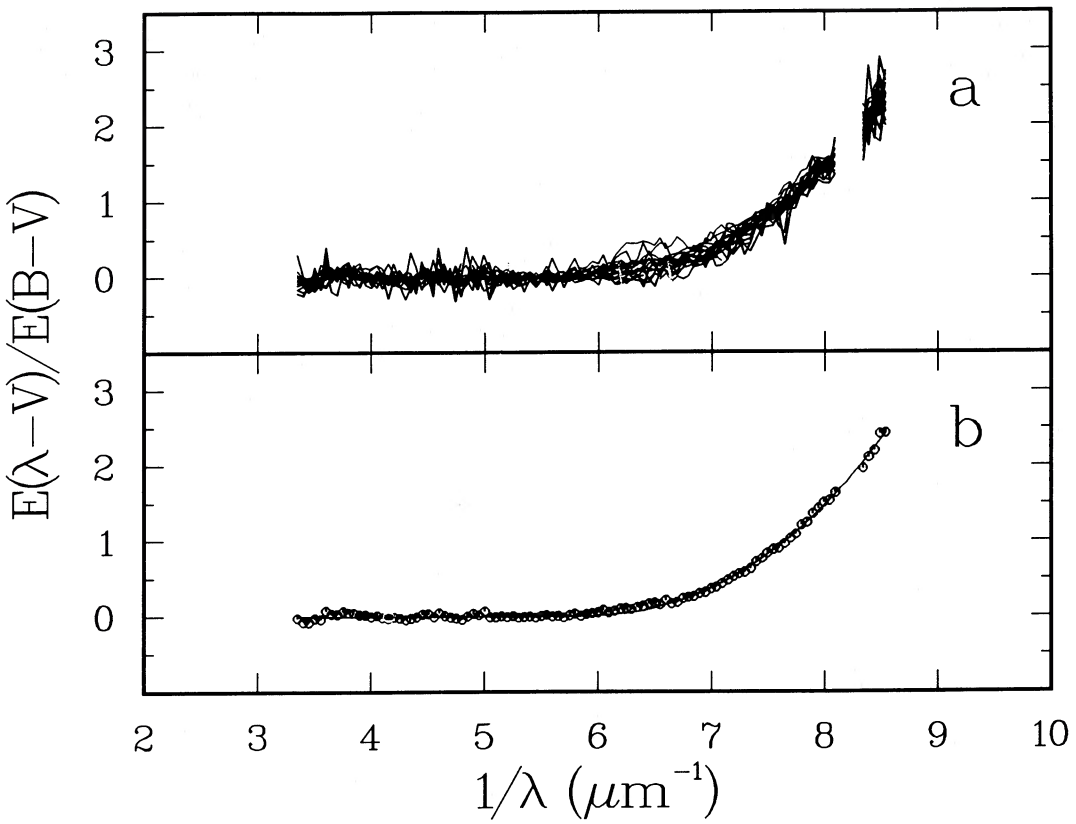

FIG. 2.—(*a*) Residual FUV curvature in 18 *IUE* extinction curves. The Drude profiles and linear background components derived in Paper I have been extrapolated out to 8.5 μm^{-1} and subtracted from the binned (in 0.05 μm^{-1} intervals) *IUE* extinction curves for the stars HD 13338, HD 14250, HD 21483, HD 36982, HD 37903, HD 46202, HD 73882, HD 147701, HD 147888, HD 147889, HD 147933, HD 154445, HD 185418, HD 239729, Herschel 36, BD +56°562, BD +60°594, and O 0936. The resultant curves, which show the residual curvature in the FUV region, were then scaled to fit the 18 curve average and are shown superposed above. (*b*) The average of the 18 individual curves from (*a*) is shown (*open circles*), along with a polynomial fit to the average (*solid line*). The parameters of the fit are given in eq. [1].

Several of the fits are shown in Figure 3. The curves have been binned as in Figure 1. The examples in Figure 3 were chosen because they illustrate nearly the full range of ultraviolet extinction properties observed in the Galaxy as well as the range in the quality of the fits to the data.

The determination of the bump parameters in the above fitting procedure differs in two respects from that in Paper I. First, the Drude profile is fitted over the entire wavelength range of the curves, rather than just the region 3.3–5.9 μm^{-1}. Second, the linear background is constrained not only by the data in the bump region, but also by the data in the FUV. The result is that the bump parameters in Table 1 differ somewhat from those derived in Paper I—chiefly because of changes in the location of the linear background. In most cases the parameters change by less than the expected measurement errors. However, for some curves the differences are larger, e.g., ζ Oph ($\gamma = 1.25$ in Paper I; $\gamma = 1.38$ in this paper), HD 93028 ($\gamma_{\rm I} = 0.77$; $\gamma_{\rm II} = 0.84$), NU Ori ($\gamma_{\rm I} = 1.00$; $\gamma_{\rm II} = 1.07$), and HD 147889 ($\gamma_{\rm I} = 1.16$; $\gamma_{\rm II} = 1.08$). Such changes are easy to understand in the shallow-bumped curves (ζ Oph, HD 93028, and NU Ori), for which the bump parameters are, in general, less well determined than in curves with strong (normalized) bumps. The HD 147889 parameters may be uncertain because the strong bump and large $E(B-V)$ value required that several different *IUE* LWR spectra, of very different exposure levels, be pieced together. The new parameters derived for this curve clearly reproduce the bump very well (Fig. 3).

It is not *a priori* obvious which fitting procedure produces the "best" bump parameters. All results presented here or in Paper I are independent of the details of the fitting process. In the present paper we adopt the self-consistent sets of parameters listed in Table 1, because they provide excellent representations of *all* the *IUE* extinction curves we have examined. The high quality of these fits leads us to conclude that the wavelength dependence of the FUV curvature in all the curves is consistent, to within the observational errors, with a single functional form.

To compare extinction curve parameters for a group of curves meaningfully, we need to know the accuracy to which they can be measured. MF give a procedure for empirically estimating the measurement uncertainties affecting various extinction parameters by using the curves derived from stars located in open clusters believed to have uniform extinction properties. We repeated their analysis using the parameterization scheme in equation (2) and the same sample of cluster stars. The resultant 1 σ uncertainties are given in Table 2. As noted in Paper I, we cannot guarantee that the cluster extinction properties are not variable at some level. Therefore, these measurement errors are understood to be upper limits.

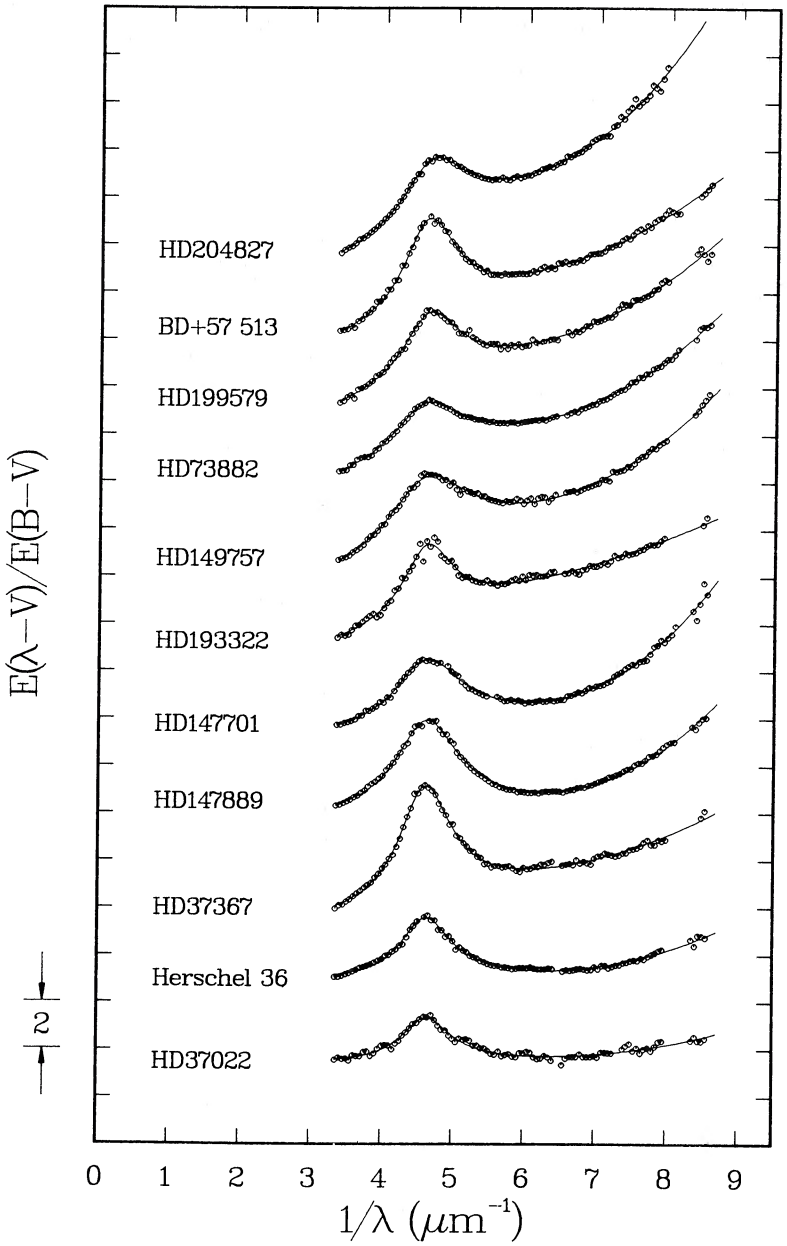

FIG. 3.—Examples of extinction curve parametrization. The binned *IUE* extinction curves for 11 stars are shown (*open circles*) with the analytical fits derived from eq. [2] superposed (*solid lines*). The coefficients of the fits are given in Table 1.

IV. EXTINCTION PARAMETER CORRELATIONS

In this section we discuss correlations among the various extinction curve parameters and between the parameters and the environments in which the extinction arises.

a) Parameter-Parameter Correlations

We have examined all 15 pairs of the six extinction curve parameters for correlations. Only pairs which showed some evidence for correlations are discussed in this section.

In Figure 4 we show a plot of c_1 (the intercept of the linear component) versus c_2 (the slope of the linear component) for the 45 curves from Table 1, along with values of the two LMC curves. All the data except the four Orion nebula stars (NU Ori, LP Ori, θ^1 Ori C, θ^1 Ori D—indicated by the small points) follow an extremely well defined linear relationship. A weighted (by $E[B-V]^2$) orthogonal least-squares fit to the data, excluding the Orion stars, is shown by the dashed line. The measurement errors for c_1 and c_2 are expected to be strongly correlated and cause data points to move in a direction nearly parallel to the linear fit. The estimated 1 σ uncertainty in the directions perpendicular and parallel to the fit, scaled to $E(B-V) = 0.55$ [the mean value of $E(B-V)$ for the 45 curve sample], are indicated by the error bars. The scatter observed about the fit is fully consistent with the expected measurement errors, while the scatter along the fit is ~ 4 times larger.

TABLE 2

EMPIRICAL UNCERTAINTIES IN EXTINCTION CURVE COEFFICIENTS

Coefficient	$\sigma \times E(B-V)$
λ_0^{-1}	0.0056
γ	0.020
c_1	0.16
c_2	0.037
c_3	0.13
c_4	0.037

The positions of the Orion curves in Figure 4*a* probably indicate problems with the extinction curves, rather than breakdown in the linear relationship between c_1 and c_2. Panek (1983) published extinction curves for LP Ori and NU Ori, as well as for other stars in the Orion nebula region. Our curves for these two stars were produced using the same data as Panek, except that Panek employed special processing to remove nebular background contamination from the *IUE* data. The first order difference between our curves for LP Ori and NU Ori and Panek's is that our curves are ~ 1.0 units and ~ 0.5 units lower in $E(\lambda - V)/E(B-V)$, respectively (indicating too much flux in the uncorrected data). Shifting our curves to match Panek's requires that their c_1 values be increased by the amounts shown by the arrows. These "corrected" values bring the points for NU Ori and LP Ori into excellent agreement with the linear relation. It is likely that the θ^1 Ori C and D curves are affected to some degree by a similar problem. This contamination probably does not seriously affect the measurement of the bump parameters. However, the slopes of the linear components should be viewed as uncertain, containing a systematic error which corresponds to the slope of the nebular background.

The linear relationship in Figure 4, which is given by $c_1 = -3.00 \times c_2 + 2.04$, demonstrates that the form of the linear component (and of the entire extinction curve) is highly constrained in the $E(\lambda - V)/E(B-V)$ versus $1/\lambda$ plane. This relationship can be used to rewrite the background extinction (which is defined as, $k_b[\lambda - V] = c_2 \times \lambda^{-1} + c_1$) in the form $k_b(\lambda - V) = c_2 \times (\lambda^{-1} - 3.00) + 2.04$. This expression for $k_b(\lambda - V)$ reveals that the linear components for all the curves can be viewed as a set of

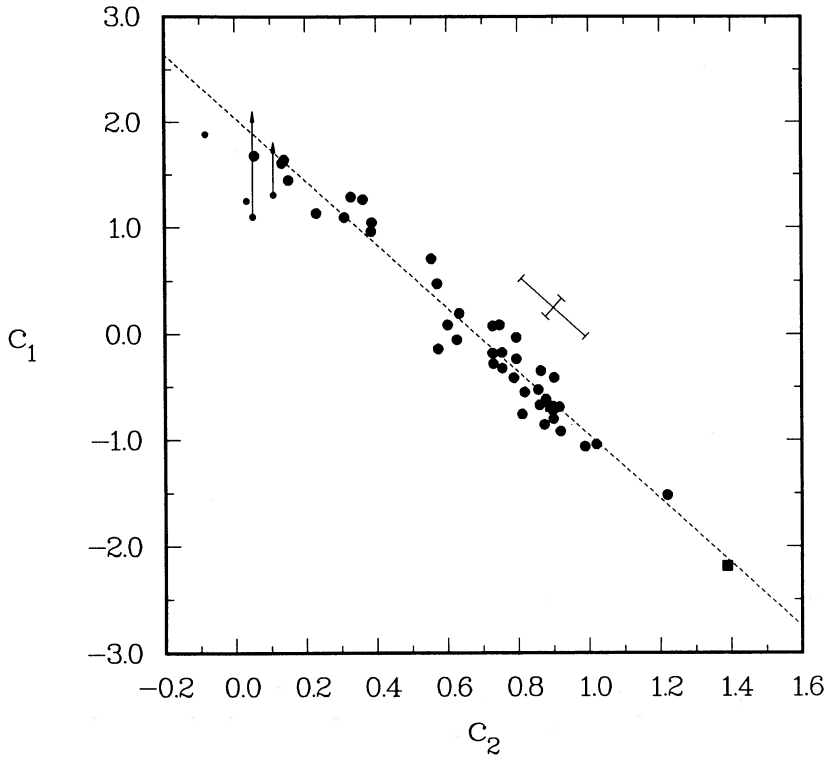

FIG. 4.—Plot of c_1 (linear component intercept) vs. c_2 (linear component slope) for the 45 individual curves listed in Table 1 (*filled circles*) and the two LMC curves (*filled squares*). The four stars located in the Orion nebula region (HD 36982, HD 37022, HD 37023, HD 37061) are indicated by the smaller circles. First-order corrections to the c_1 values of HD 36982 and HD 37061, resulting from nebular contamination of the *IUE* data, are shown by the arrows. Similar corrections are likely to apply to the HD 37022 and HD 37023 data. The dashed line shows an orthogonal, weighted [by $E(B-V)^2$] linear least-squares fit to the 45 curve sample, excluding the Orion stars. The equation of the fit is, $c_1 = -3.00 \times c_2 + 2.04$. Errors in c_1 and c_2 are strongly correlated. The 1 σ error bars, scaled to $E(B-V) = 0.55$, in the directions parallel to and perpendicular to the fit are shown.

lines with different slopes radiating from the point $E(\lambda - V)/E(B-V) \approx 2$ at $\lambda^{-1} = 3\ \mu m^{-1}$. This relationship reduces the number of free parameters required to describe the curves properties from six to five.

We now search for possible relationships involving the bump parameters. (Plots involving λ_0^{-1} are not presented because its variability is too small to be useful for seeking relationships with other parameters.) Bump strength parameters, such as c_3 or the bump area, and continuum parameters such as c_1, c_2, and c_4 can be directly compared. Because they are all scaled by $E(B-V)$, any mutual dependence will simply be scaled by this choice of normalization and not otherwise affected. Figure 5 is a plot of the FUV curvature, c_4, versus the Drude coefficient c_3. Different symbols represent different bump widths. The important thing to notice in Figure 5 is that progressing from the lower left to the upper right of the diagram, the points fan out and the value of γ increases. The one obvious exception to this trend is the point for NU Ori. However, the γ measurement for this star is suspect for two reasons. First, because it has a very weak bump, its γ value is poorly determined by the fitting procedure. Second, it is the only Orion star whose curve has a $\gamma > 0.9$. It would be useful to verify this measurement.

Figure 6*a* is a plot of c_4 versus γ. A well-defined correlation exists. Its interpretation is not straightforward because c_4 is scaled by $E(B-V)$, while γ is scale-free. Figure 6*b* is a similar plot of the bump strength, c_3, versus γ which also exhibits a well-defined correlation. Recall that measures of bump strength and γ must be related at some level and that other reasonable bump strength measurements, such as bump area or central intensity, are more poorly related to γ (see MF). A possible explanation for both of the relationships seen in Figure 6 is discussed in § V.

Extreme care must be taken when examining relationships between the FUV curvature component c_4 and parameters which describe the 2175 Å bump. Because the Drude function contributes to the curvature of the fit well into the FUV, there can be significant interplay between the bump parameters and the FUV curvature parameter arising solely from the fitting procedure. For example, if the actual structure of the bump differs significantly from a Drude profile in the FUV, then the FUV component would have to make up the difference in the least-squares fit. Furthermore, for fixed bump strengths, fits with wider bumps contribute more strongly to the FUV curvature—this is the sense of the effect seen in Figures 5 and 6*a*.

We estimated the magnitude of the connection between c_4 and γ by fitting the blue tail ($\lambda^{-1} > 5.9\ \mu m^{-1}$) of the Drude profile by a combination of the linear and FUV components. This was done for γ's of 0.8 and 1.2, which represent the extreme range of the sample. Although the c_4 coefficient does change, its maximum change is only 0.077 for a c_3 of 3.5, which is typical for our sample. The magnitude of the effect is shown by the vertical arrows in Figure 5 and is seen to be smaller than the observational error. Thus, there appears to be a real correlation present, in the sense that curves with broader bumps have stronger FUV curvature. This relationship suggests the possibility that, at least for the broadest bumps, the FUV curvature and the bump width are related.

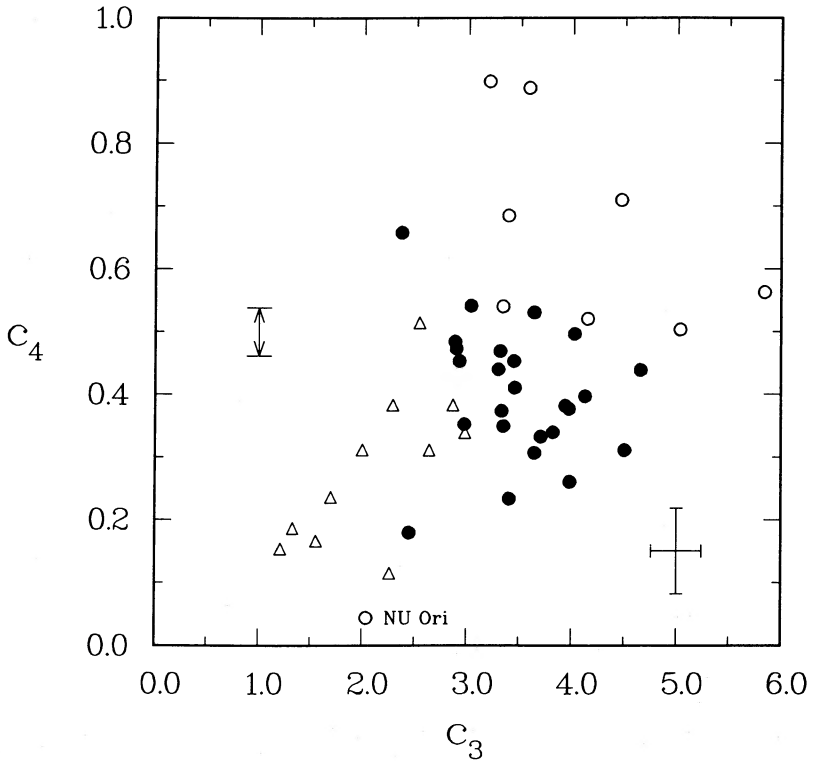

FIG. 5.—Plot of c_4 (FUV curvature scale factor) vs. c_3 (Drude profile scale factor) for the 45 individual curves listed in Table 1. Different symbols represent different ranges in the value of the bump width parameter γ: *open triangles*, $\gamma \leq 0.90$; *filled circles*, $0.9 < \gamma < 1.05$; *open circles*, $\gamma \geq 1.05$. Vertical arrows indicate the maximum effect on the measurement of c_4 due to the assumption that the shape of the 2175 Å bump can be extrapolated into the FUV using the Drude profile. The 1 σ error bars for c_3 and c_4, scaled to $E(B-V) = 0.55$, are shown.

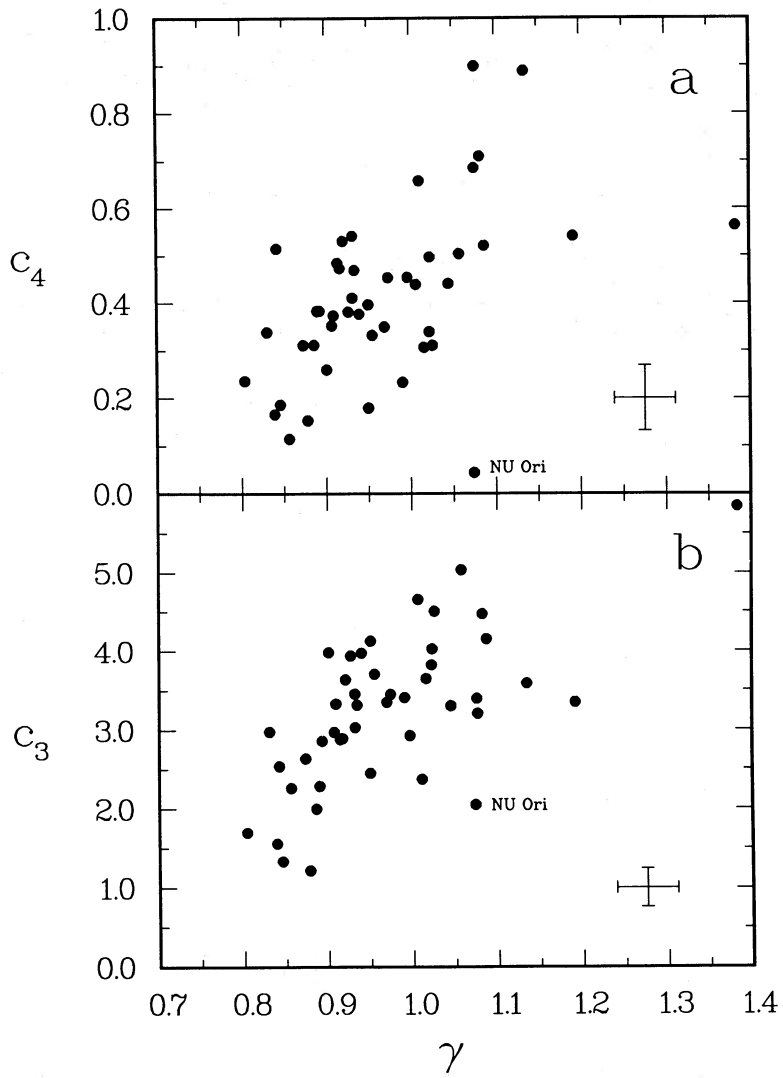

FIG. 6.—(*a*) Plot of c_4 (FUV curvature scale factor) vs. γ (bump width parameter) for the 45 individual curves listed in Table 1. The 1 σ error bars for c_4 and γ, scaled to $E(B-V) = 0.55$, are shown. (*b*) Same as (*a*) for c_3 (Drude profile scale factor) vs. γ.

b) Environmental Correlations

Following Massa, Savage, and Fitzpatrick (1983) and Paper I, we make a crude separation of our data sample into a "dense medium" group and a "diffuse medium" group. A special subset of the dense medium group includes the lines of sight to the Trapezium stars θ^1 Ori C and D and Herschel 36, which pass through regions of recent early-type star formation. The environment type for each of the 45 stars in our primary sample is given in Table 1, column (5).

We found in Paper I that the bump parameters A (normalized bump area) and λ_0^{-1} (location of bump peak) are insensitive to this environmental breakdown. The FWHM γ, however, showed a strong environmental correlation, with a correlation coefficient of 0.72. Bumps in the dense medium group tend to be broad, and those in the diffuse regions and in the early-type star formation regions tend to be narrow.

Plots of c_2 (linear component slope) and c_4 (FUV curvature strength) versus $E(B-V)/r$ are shown in Figure 7. The open, half-filled, and filled symbols represent the dense medium curves, the Trapezium and Herschel 36 curves, and the diffuse medium curves, respectively. Note that $E(B-V)/r$ itself is not always an accurate discriminator between the dense and diffuse lines of sight, but it provides a convenient format for examining environmental effects.

Figure 7*a* shows a strong separation between the two environmental groups. Although the dense group curves show a wide range of slopes, all curves with $c_2 < 0.5$ are dense medium curves. The diffuse medium curves do not exhibit nearly as much variability in c_2 and their slopes tend to be higher on average.

Figure 7*b* shows that the strength of the FUV curvature component is not a strong function of our environmental breakdown, although, as with Figure 7*a*, the dense medium curves show a wider range of variability than the diffuse group. The average value of c_4 for the dense group curves is slightly greater than for the diffuse medium curves.

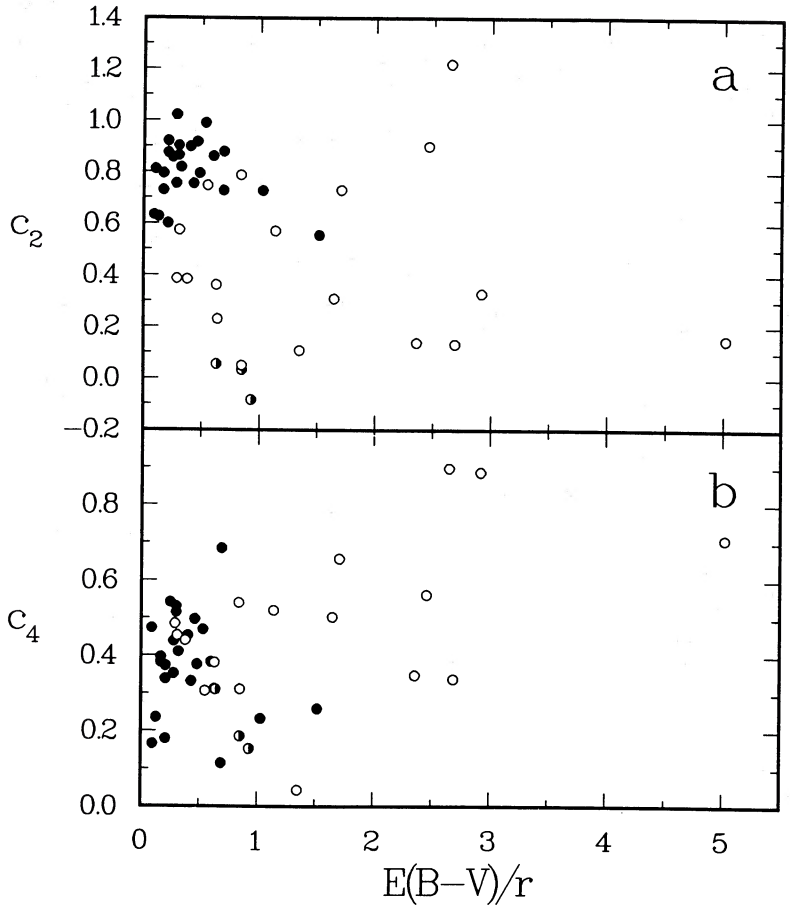

FIG. 7.—(*a*) Plot of c_2 (linear component slope) vs. $E(B-V)/r$ (a crude dust density indicator). The different symbols represent lines of sight passing through the diffuse interstellar medium (*filled circles*), through dense clouds (*open circles*), and through regions of recent early-type star formation (*half-filled circles*). The point with the largest value of $E(B-V)/r$ (~ 5) represents the star HD 147889. (*b*) Same as (*a*) for c_4 (FUV curvature scale factor) vs. $E(B-V)/r$.

V. DISCUSSION

Ultimately, one would like to identify some combination of the functions which describe the curves with the cross sections of different constituents or properties of the dust. Unfortunately, all analyses like the one presented here are necessarily ambiguous and strongly dependent upon the adopted set of fitting functions. For example, it is possible to take the individual fitting functions to represent specific extinction properties of different constituents of the dust. On the other hand, we could just as well have started with any set of linear combinations of these and interpreted the data in terms of this set. However, several factors suggest that the situation is not quite so arbitrary. For one thing, the signature of the 2175 Å bump is very distinct and very well represented by a Drude profile, which also has a strong physical basis. This provides a firm starting point for subsequent curve decomposition. In addition, the resulting set of fitting functions (i.e., a Drude profile, a linear term, and a simple polynomial curvature term) are all representative of the shapes of cross sections of actual materials thought to be present in interstellar dust (see, e.g., Draine and Lee 1984).

The relationship between c_1 and c_2 (the coefficients of the linear component) suggests that only five parameters are actually necessary to describe all of the observed curves. The interpretation of this result is helpful in illuminating the preceding remarks because it can be interpreted in two equally acceptable ways. One is that a particular component of the grain population constitutes a one-parameter family of extinction properties, and, as the parameter changes, the ultraviolet slope of the resulting curve also changes. Evolutionary processes, such as shock processing of silicates (Seab and Shull 1983), could produce a family of extinction curves with different ultraviolet slopes which follow the relationship shown in Figure 4. An alternative interpretation is that there are two or more distinct grain populations which produce different ultraviolet extinction slopes. Intermediate slopes would then result from different mixtures of these populations along different lines of sight. Such an interpretation is suggested by the three-component model of the interstellar medium proposed by Spitzer (1985) to explain observed depletion patterns. The dust from one of these components would have to cause nearly gray FUV extinction (resembling the classical van de Hulst grains; van de Hulst 1957) in order to produce curves such as those of the Trapezium stars or HD 147889 (see Fig. 3). The dust from another component must cause extinction which is nearly linear throughout the visual and UV (resembling the astronomical silicates discussed by Draine and Lee 1984) in order to produce curves like those for HD 204827 and HD 193322. In reality, certain aspects of both of these interpretations probably contribute to the observed relationship.

Another important point concerning the linear "background" is that its dispersion is much smaller for the diffuse curves than for

the dense region curves (Fig. 7). This is in spite of our sample bias toward peculiar extinction curves and probably reflects the fact that conditions are much more uniform in the diffuse interstellar medium.

For the bump, the decomposition is somewhat less ambiguous because we are fairly certain that we are measuring the concentration of a particular constituent of the dust. However, even in this case we cannot recover the entire functional form of the extinction caused by this material. This is because we cannot identify what portions of the other functional components, such as the linear background, are also attributed to the cross section of the bump-producing particles. In general, it is impossible to determine how much of a "background" curve is associated with a given feature unless we can identify as many features as there are degrees of freedom in a background. Nevertheless, some clues are available. One is the observation that the curve for HD 147889 has a strong bump and essentially zero slope. Another is that there is a total lack of correlation between either c_1 or c_2 and any of the bump parameters. Both of these observations agree with the Greenberg and Chlewicki (1983) result that very little of the linear extinction is associated with the bump material, although it is quite possible that some UV-gray component is associated with it.

The systematic behavior of the FUV curvature has received less attention than the other aspects of the curves. Massa, Savage, and Fitzpatrick (1983) observed that their mean "dense environment" curve seemed to have more FUV curvature and a broader bump than their mean diffuse medium curve but did not pursue the point. Greenberg and Chlewicki (1983) were the first to study the FUV curvature systematically. For a sample of diffuse medium curves, they found that the shape of FUV extinction from 5.88–7.69 μm^{-1} did not vary, and attributed it to a single extinction component present in varying amounts in the curves. In contrast, we have found that two distinct and uncorrelated components (the linear and FUV curvature components) are required to understand the observed shapes of extinction curves in the FUV. This apparent conflict can be resolved by considering the samples and normalization procedures. Inspection of Figure 6 shows that neither the slope nor the FUV curvature vary strongly for the diffuse medium stars. Consequently, since Greenberg and Chlewicki's diffuse medium curves are normalized between 5.88 and 7.69 μm^{-1}, little variability would be expected. The magnitude of the variability, and the requirement for two distinct components, do not become apparent untile the dense region curves are incorporated into the sample. Specific comparison of a few dense and diffuse medium curves makes the lack of correlation between the components obvious. For example, the curves for HD 147889 and HD 37367 (see Fig. 3) both have very small linear slopes but large and small FUV curvature, respectively. Similarly, HD 204827 and HD 193322 both have strong linear slopes but large and small FUV curvature, respectively. Such an extreme lack of correlation is indicative of extinction features arising from two distinct populations of grains. Consequently, it would appear that the grains responsible for the linear ultraviolet slope and the FUV curvature belong to separate populations.

The fact that the shape of the FUV curvature is the same in all of the observed curves (Fig. 2), regardless of either their environment or the shape of the rest of the curve, suggests that it is not simply an artifact of the size distribution or relative amounts of the absorbing particles, but rather a distinct optical property of some physical component of the dust.

Although the data on the dependence of FUV curvature on γ (Fig. 5) are not adequate to draw any definitive conclusions, they do suggest an enticing possibility. This is that the FUV curvature is actually the red wing of a second particle resonance which is broadening in step with the 2175 Å resonance. Such an interpretation is plausible for two reasons. First, the shape of the FUV curvature resembles the wing of a Drude profile. Second, Hecht (1986) has pointed out that small (radii < 100 Å) graphite-like grains are expected to have two plasmon resonances, one which produces the 2175 Å bump, and another which produces an absorption bump centered in the FUV between 700 and 800 Å, similar to that seen in pure graphite (see Draine and Lee 1984). Thus, there are physical grounds to expect that the FUV curvature is the red wing of a second resonance.

If both the 2175 Å bump and the FUV curvature are due to resonances dominated by absorption in the same population of particles, then, for a given mass column density, M, the absorption profile of each resonance is proportional to (Bohren and Huffman 1983) $\gamma M\lambda_0^{-2}D(\lambda^{-1}, \gamma, \lambda_0^{-1})$, where M, λ_0, and γ refer to the particular resonance under consideration and will be distinguished by "FUV" and "2175" whenever confusion may arise. Within the framework of this simplistic interpretation, the quantities c_3 and c_4 (which are normalized by $E[B-V]$ are, to first order, proportional to $\gamma M/[\lambda_0^2 E(B-V)]$. This gives a plausible physical basis for why c_3 is the bump strength measure which is most strongly correlated with γ (Fig. 6*b*). Furthermore, the $c_4 - \gamma$ relationship can be given the following interpretation. Because c_4 is proportional to $\gamma(\mathrm{FUV})M(\mathrm{FUV})/[\lambda_0(\mathrm{FUV})^2 E(B-V)]$ and correlates well with $\gamma(2175)$, the natural explanation is that $\gamma(\mathrm{FUV})$ scales in the same way as $\gamma(2175)$, and that $M(\mathrm{FUV})/[\lambda_0(\mathrm{FUV})^2 E(B-V)]$ is relatively constant for all lines of sight. On the other hand, the wedge shape of the $c_3 - c_4$ diagram (Fig. 6*a*) implies that $M(\mathrm{FUV})/[\lambda_0(\mathrm{FUV})^2 E(B-V)]$ and $M(2175)/\lambda_0(2175)^2 E(B-V)]$ are not well correlated, and that the correlation becomes progressively worse as $\gamma(2175)$ increases. It is possible that this behavior indicates that $M(2175)$ and $M(\mathrm{FUV})$ are poorly coupled in curves with large γ's, which also correspond to denser regions. Since Hecht's (1986) model predicts that hydrogenation of carbon grains will effectively decouple the 2175 Å and FUV resonances, and because dense regions correspond to those in which hydrogenation of the carbon grains would be most likely to occur, these results are in qualitative agreement with Hecht's model.

Another explanation for the $c_4 - \gamma$ relationship is that even though γ and c_4 are due to two distinct and unrelated grain populations, the optical properties of both populations respond to a single environmental factor in the same way. Consequently, the relationship between the two is only apparent, arising solely from the fact that both sets of particles are responding to a common physical agent. However, the fact that the FUV curvature is essentially independent of environment (Fig. 7*b*), while γ is strongly dependent upon environment (Fig. 4*c* in Paper I), argues against this interpretation. In fact, we see that the FUV curvature and γ are related in spite of the environmental influences affecting γ. If, however, more than one physical factor is influencing the observed behavior, then the preceding argument is not valid.

Because of its potential importance to our physical understanding of interstellar grains, the reality of the $\gamma - c_4$ relationship must be more firmly established. Clearly, observations of lines of sight with extremely narrow or broad bumps would be most useful in this regard. An analysis of lines of sight with broad bump extinction curves would be especially important in another context.

Because curves with broad bumps show the largest variance in FUV curvature for fixed bump width, an analysis of such curves would be most likely to reveal which additional factors may be influencing γ or c_4. Observations of stars suspected to have extremely broad or narrow bumps are currently under way.

This work was supported by NASA grant NAG5-78.

REFERENCES

Bless, R. C., and Savage, B. D. 1972, *Ap. J.*, **171**, 293.
Boggess, A., *et al.* 1978*a*, *Nature*, **275**, 372.
———. 1978*b*, *Nature*, **275**, 377.
Bohlin, R. C. 1975, *Ap. J.*, **200**, 402.
Bohlin, R. C., and Savage, B. D. 1981, *Ap. J.*, **249**, 109.
Bohren, C. F., and Huffman, D. R. 1983, *Absorption and Scattering of Light by Small Particles* (New York: Wiley-Interscience).
Draine, B. T., and Lee, H. M. 1984, *Ap. J.*, **285**, 89.
Fitzpatrick, E. L. 1986, *Ap. J.*, **92**, 1068.
Fitzpatrick, E. L., and Massa, D. 1986, *Ap. J.*, **307**, 286 (Paper I).
———. 1988, in preparation (Paper III).
Greenberg, J. M., and Chlewicki, G. 1983, *Ap. J.*, **272**, 563.
Hecht, J. 1986, *Ap. J.*, **305**, 817.
Hecht, J., Helfer, H. L., Wolf, J., Donn, B., and Pipher, J. L. 1982, *Ap. J. (Letters)*, **263**, L39.
Massa, D., and Fitzpatrick, E. L. 1985, *Ap. J. Suppl.*, **60**, 305 (MF).
Massa, D., Savage, B. D., and Fitzpatrick, E. L. 1983, *Ap. J.*, **266**, 662.
Morgan, D. H., McLachlan, A., and Nandy, K. 1982, *M.N.R.A.S.*, **198**, 779.
Panek, R. J. 1983, *Ap. J.*, **270**, 169.
Seab, C. G. 1982, Ph. D. thesis, University of Colorado.
Seab, C. G., and Shull, J. M. 1983, *Ap. J.*, **275**, 652.
Seaton, M. J. 1979, *M.N.R.A.S.*, **187**, 73P.
Spitzer, L. 1985. *Ap. J. (Letters)*, **290**, L2.
van de Hulst, H. J. 1957, *Light Scattering by Small Particles* (New York: Wiley).
Witt, A. N., Bohlin, R. C., and Stecher, T. P. 1984, *Ap. J.*, **279**, 698.

EDWARD L. FITZPATRICK: Princeton University Observatory, Peyton Hall, Princeton, NJ 08544

DERCK MASSA: Applied Research Corporation, 8201 Corporate Drive, Suite 920, Landover, MD 20785